

Dependence of Transmission Curves on Input Optical Power in an Electroabsorption Modulator

Jongin Shim, *Member, IEEE*, Bin Liu, and John E. Bowers, *Fellow, IEEE*

Abstract—We present a novel method to extract the optical absorption coefficient of a semiconductor electroabsorption modulator (EAM) with antireflection coated facets. Only the transmission and photocurrent data are needed with this method. The method allows to obtain the total optical coupling loss, internal quantum efficiency, and optical absorption coefficients when input optical power is low. We also developed a method to analyze optical absorption coefficient with the saturation effect. By using those methods, we investigated the dependence of the transfer curves on the input optical power in a multiple-quantum-well EAM. The optical loss saturation effect and the increase of device temperature are the dominant mechanisms for the dependence of transfer curves on the input optical power in the low bias region and the high bias region, respectively.

Index Terms—Electroabsorption modulator, optical loss, photocurrent, saturation, temperature.

I. INTRODUCTION

SEMICONDUCTOR electroabsorption modulators (EAMs) are widely considered for the use in analog and digital optical communication links. In digital links, high extinction ratio, low driving voltage, and low chirp are major concerns [1], [2]. In analog links, high spurious free dynamic range (SFDR), high link gain (G), and low noise figure (NF) are desirable [3]. These link performances are mainly determined by the modulator transfer characteristics. The modulator transfer function is defined by the optical transmission versus the applied bias voltage. EAMs have excellent properties such as their small size, large bandwidth, low driving voltage, high extinction ratio, and potential for monolithic integration with other semiconductor components [1]–[3]. However, an EAM shows a complicated nonlinear transfer function and it has a strong dependence on input optical power [4]. These make it difficult to obtain high gain and low noise figure in an optical link. Thus, it is essential to physically understand transfer function of an EAM for the realization of a high-performance optical link.

The previous reports show that most modulators based on the quantum confined Stark effect (QCSE) suffer a large insertion loss ranging from 6 to 12 dB even at zero bias voltage [4]. The insertion loss consists of coupling loss to optical fibers, waveguide scattering and radiation losses, and the residual interband

absorption loss. Those various losses play different roles on the nonlinear behavior of transfer curve in an EAM. For the purposes of material characterization and device optimization, it is valuable to separate those different optical losses and to clarify the reasons of the input optical power dependency of transfer curves.

A number of methods have been reported for the determination of the optical gain/loss in a waveguide device. Most of them are based on the Fabry–Perot (FP) resonance spectra and their Fourier analysis [5]–[7]. In order to apply these methods, an EAM should have finite facet reflections as well as low propagation loss such that the peaks and valleys of individual FP resonance can be discriminated. In usual case, the facets of an EAM are coated with antireflection (AR) films for high light coupling. Even with cleaved facets, the residual loss $\alpha_{cv}(V_B = 0)$, namely an interband absorption loss at zero bias is not negligible since QCSE is only effective near the exciton resonance energy. Therefore, the resonances of an EAM are hardly observed at operation wavelength so that the conventional methods are not adequate to estimate the absorption coefficient of an EAM. A direct optical loss measurement method based on photocurrent and transmission was proposed by Wood [8]. In this approach, a waveguide scattering loss and radiation loss α_i is assumed and then the residual loss $\alpha_{cv}(V_B = 0)$ is deduced. However, the value of $\alpha_{cv}(V_B = 0)$ is very sensitive to the guessed value of α_i . Chin improved Wood's method with the assumption of α_i is negligibly small compared to the interband absorption $\alpha_{cv}(V_B)$ at high bias level V_B [9]. Therefore, the previous reports have a difficulty to distinguish the waveguide optical loss α_i from the total unsaturated optical loss $\alpha_{tot,u}(V_B) (= \alpha_i + \Gamma\alpha_{cv})$ where Γ is the optical confinement factor in multiple quantum wells (MQWs), which in turn makes it difficult to know the waveguide coupling loss directly. $\alpha_{tot,u}(V_B)$ indicates the total propagation optical loss of an EAM when optical input power is very small and it has little dependence on both the optical intensity and the longitudinal position z inside an EAM.

In this paper, we improve the previous methods to extract optical losses of an EAM with AR-coated facets for a small optical input power. It leads to find unsaturated values of the optical coupling loss between light source and EAM, photocurrent conversion efficiency η_i , waveguide scattering loss α_i , and interband absorption coefficient α_{cv} separately. For a high input optical power, we introduce a phenomenological absorption coefficient with saturation effects which is able to know the longitudinal dependence of absorption coefficient in an EAM. Finally, the dependence of optical transmission curves on optical input powers is clarified theoretically and experimentally.

Manuscript received April 19, 2004; revised July 9, 2004.

J. Shim is with the Department of Electrical and Computer Engineering, Hanyang University, Kyungki-do 425-791, Korea (e-mail: jishim@giga.hanyang.ac.kr).

B. Liu is with LuminentOIC Inc., Chatsworth, CA 91311 USA.

J. E. Bowers is with the Department of Electrical and Computer Engineering, University of California, Santa Barbara, CA 93106 USA.

Digital Object Identifier 10.1109/JQE.2004.835115

II. OPTICAL ABSORPTION COEFFICIENTS

The physical mechanism of an EAM is that an applied electric field shifts the absorption peak toward lower photon energies based on either the Franz–Keldysh (FK) or QCSE. The modulation involves the creation of electron-hole pairs inside the quantum wells. These created carriers in turn may or may not change the electric field and the absorption coefficient in the quantum wells [10].

When the total number of photogenerated carriers is small enough and an electric field is sufficient to sweep out photo-generated carriers, the optical absorption coefficient may be independent of an input optical intensity and have the same value along the propagation direction in an EAM. This unsaturated optical absorption coefficient results from several optical absorption processes such as waveguide scattering loss α_{sc} , free carrier absorption α_{fc} , intervalence band absorption α_{IVBA} , and interband absorption between the conduction band and the valence band α_{cv} . α_{sc} and α_{fc} come from the waveguide roughness and the plasma effect of the carriers, respectively. α_{IVBA} occurs dominantly between the heavy-hole band and the spin-split band in InGaAsP material systems [11]. Optical losses due to α_{sc} , α_{fc} , and α_{IVBA} can reduce the photon number, but make no contributions to generate electron-hole pairs. We represent optical losses that do not generate the photocurrent as the intrinsic optical loss coefficient of α_i . Since an EAM is usually operated under the reverse bias, it is expected that α_{fc} and α_{IVBA} are not significant compared to α_{sc} . In this case, α_i can be considered as a constant regardless of applied bias voltages.

The interband optical loss coefficient α_{cv} stands for optical losses generating electron-hole pairs. Thus, the carriers generated only by α_{cv} process can contribute the photocurrent generation. When the negligible number of created carriers exists in the well, α_{cv} is affected by the externally applied bias voltage as well as the internally generated carriers itself. Excitonic saturation, bandgap shrinkage, and the electric field screening are the known reasons for the saturated optical absorption coefficient [12]–[15]. Excitonic saturation represents a bleaching of the exciton absorption peak due to many-body effects, such as scattering and screening. Bandgap shrinkage is caused by many-body effects as well as by temperature increase. The photogenerated carriers screen the externally applied electric field, which in turn induces a change of the absorption through the QCSE. Charge buildup inside the quantum wells due to differential escape rates of electrons and holes can lead to an inhomogeneous electric field in the intrinsic region.

In this paper, we will first describe a new method to extract the unsaturated optical absorption coefficient and then extend it to the saturated situation.

A. Unsaturated Optical Absorption Coefficient

First, we consider the case that α_i and α_{cv} are uniform inside an EAM. This assumption is reasonable when optical intensity is low enough that the carrier band filling has a negligible effect on absorption processes. We can formulate the following equations for the optical transmission and the photocurrent using the

absorption coefficients discussed above [16], [17]. The propagation of an optical power and the photocurrent in an electroabsorption modulator can be described by the following equations:

$$dP = -(\alpha_i + \Gamma\alpha_{cv})P(z) dz \quad (1)$$

$$dI_{ph} = -(q/h\nu)\eta_i\Gamma\alpha_{cv}P(z) dz \quad (2)$$

where dP and dI_{ph} are the changes of optical power and generated photocurrent between $z \sim z+dz$ along z -direction, respectively. q , $h\nu$, and Γ are the electron charge, an incident photon energy, and the optical confinement factor in MQWs. $P(z)$ is the optical power at the position z . $\eta_i(V_B)$, the photocurrent conversion efficiency, is defined as the number of electron-hole pairs contributing to photocurrent per the number of electron-hole pairs generated by photons, which is the same as Wood's definition of the internal quantum efficiency [8]. Since a part of photogenerated carriers will be trapped at the hetero-interface and recombined before escaping the hetero-barriers, $\eta_i(V_B)$ will be low at low bias voltage V_B [18]. But when the voltage applied to the device is sufficient to sweep out all the carriers, $\eta_i(V_B)$ will be constant as approximately unity. The boundary conditions for (1) and (2) are

$$P(z = 0^+) = P_{in}C_{input}(1 - R_f) \quad (3)$$

$$P_{out} = P(z = L^-)(1 - R_f)C_{output} \quad (4)$$

where L and R_f are the modulator length and the facet power reflectivity, respectively. $z = 0^+$ and $z = L^-$ represent the end positions inside the modulator at the input and the output ports, respectively. P_{in} and P_{out} are the optical powers at the input port and the output port, respectively. C_{input} and C_{output} are the optical coupling efficiencies at the input and the output ports, respectively.

The analytical solutions of (1) and (2) are given by

$$T(V_B) = P_{out}/P_{in} = K_p e^{-\alpha_i L} e^{-\Gamma(\alpha_{cv,o} + \Delta\alpha_{cv})L} \quad (5)$$

$$I_{ph}(V_B) = K_h P_{in} \frac{\Gamma(\alpha_{cv,o} + \Delta\alpha_{cv})}{\alpha_i + \Gamma(\alpha_{cv,o} + \Delta\alpha_{cv})} \times \left\{ 1 - e^{-\alpha_i L} e^{-\Gamma(\alpha_{cv,o} + \Delta\alpha_{cv})L} \right\} \quad (6)$$

where T and $I_{ph}[mA]$ represent the transmission and the photocurrent generated in an EAM, respectively. $\alpha_{cv,o}$ denotes $\alpha_{cv}(V_B = 0)$ which corresponds to the residual optical loss due to the interband absorption and $\Delta\alpha_{cv}(V_B) = \alpha_{cv}(V_B) - \alpha_{cv}(0)$ is the optical loss change at a bias voltage V_B . The constants K_p and K_h represent as

$$K_p = C_{input}C_{output}(1 - R_f)^2 \quad (7)$$

$$K_h = (q/h\nu)\eta_i C_{input}(1 - R_f). \quad (8)$$

By combining (5) with (6), the photocurrent I_{ph} can be rewritten as follows:

$$\frac{I_{ph}(V_B)}{1 - e^{-\alpha_i L} e^{-\Gamma\alpha_{cv,o} L} T_n(V_B)} = b - \frac{c}{a - \ln T(V_B)} \quad (9)$$

where

$$T_n(V_B) = \frac{T(V_B)}{T(0)} \quad (10)$$

$$a = \ln(K_p) = \ln\{C_{\text{input}}C_{\text{output}}(1 - R_f)^2\} \quad (11)$$

$$b = K_h P_{\text{in}} = \eta_i(V_B)(q/h\nu)C_{\text{input}}(1 - R_f)P_{\text{in}} \quad (12)$$

$$c = (\alpha_i L)(K_h P_{\text{in}}). \quad (13)$$

Equation (9) is the key equation to find an unsaturated optical absorption loss. In the following analysis, η_i is assumed as a constant when an applied bias voltage is greater than V_{min} , where the intrinsic absorption region is completely depleted. The minimum applied bias voltage V_{min} can be deduced from the previous reports [8], [9]. Here, we choose V_{min} as the voltage where the normalized optical transmission T_n reaches less than about -6 dB.

Next, we will explain the analysis procedure of our proposed method. At first, the analysis is done for $V_B \geq V_{\text{min}}$. We assume α_i and $\Gamma\alpha_{\text{cv},o}$. The left term $f_l(V_B)$ in (9) is calculated by using measured data of $I_{\text{ph}}(V_B)$ and $T_n(V_B)$. Next, $f_l(V_B)$ is plotted as a function of $\ln T(V_B)$ in order to fit the expression shown in the right term of (9). The constants a , b , and c are extracted from the data set of $(f_l, \ln T)$. Then, K_p , K_h , and α_i are calculated from the extracted values of a , b , and c . We know from (5) and (6) that

$$\Gamma\Delta\alpha_{\text{cv}}(V_{\text{min}}) = -(1/L)\ln(T_n(V_{\text{min}})) \quad (14)$$

$$\Gamma\alpha_{\text{cv},0} = \frac{1}{L}\ln\left(\frac{K_p}{T(V_{\text{min}})}\right) \frac{I_{\text{ph}}/K_h P_{\text{in}}}{1 - T(V_{\text{min}})/K_p} - \Gamma\Delta\alpha_{\text{cv}}(V_{\text{min}}). \quad (15)$$

Equations (14) and (15) provide the new value of $\Gamma\alpha_{\text{cv},o}$. We compare that the obtained values of α_i and $\Gamma\alpha_{\text{cv},o}$ to initially assumed ones. If the errors are negligibly small, then we stop the iteration procedure. Otherwise, we repeat the calculation procedure with the new values of α_i and $\Gamma\alpha_{\text{cv},o}$ as initial values. After the iteration in the range of $V_B \geq V_{\text{min}}$, the constant values of $C_{\text{input}}C_{\text{output}}$, $C_{\text{input}}\eta_i$, α_i , and $\Gamma\alpha_{\text{cv},o}$ are known. The measured data of $I_{\text{ph}}(V_B)$ and $T(V_B)$ are used in order to find $\Gamma\alpha_{\text{cv}}(V_B)$ and $C_{\text{input}}(1 - R_f)\eta_i(V_B)$ for all applied bias voltages.

Even though our method gives correct values of $C_{\text{input}}(1 - R_f)\eta_i$ for $V_B \geq V_{\text{min}}$, it doesn't allow to know the values of C_{input} and $\eta_i(V_B)$ separately. But $\eta_i(V_B)$ can be assumed as nearly one for $V_B \geq V_{\text{min}}$ since the applied electric field is sufficient to sweep out all photogenerated carriers. R_f is also neglected for an EAM with AR film-coated facets. In these situations, C_{input} and $\eta_i(V)$ are found separately from the extracted value of b and (6). The photocurrent conversion efficiency $\eta_i(V_B)$ is expressed as

$$\eta_i(V_B) = \frac{h\nu}{q} \left(\frac{\alpha_{\text{tot},u}}{\Gamma\alpha_{\text{cv}}} \right) \frac{I_{\text{ph}}(V_B)}{C_{LD-m}(1 - R_f)P_{\text{in}}(1 - e^{-\alpha_{\text{tot},u}L})} \quad (16)$$

where $\alpha_{\text{cv}} = \alpha_{\text{cv},o} + \Delta\alpha_{\text{cv}}$ and $\alpha_{\text{tot},u} = \alpha_i + \Gamma\alpha_{\text{cv}}$.

B. Saturated Optical Absorption Coefficient

When an optical input power is strong enough, both space charge buildup and exciton saturation effects are not negligible. In this case, the absorption coefficient will have a strong longitudinal distribution. In order to include the longitudinal dependence of optical absorption coefficient, we assume a phenomenological absorption saturation dependence of the form at a first approximation [19]

$$\alpha_{\text{tot}}(V_B, z) = \frac{\alpha_{\text{tot},u}(V_B)}{1 + P(V_B, z)/P_s(V_B)}, \quad \text{where } 0 < z < L. \quad (17)$$

$\alpha_{\text{tot},u}(V_B)$ represents the total absorption coefficient at a low power and it is a constant within the modulator. In this analysis, we use an unsaturated value shown in part A. The optical power $P(V_B, z)$ is the local power inside the sample. The local power $P(V_B, z)$ is described by

$$dP = -\frac{\alpha_{\text{tot},u}(V_B)}{1 + P/P_s} P dz \quad (18)$$

and its solution is given by

$$\ln\left\{\frac{P(V_B, z)}{P(0^+)}\right\} = -\frac{P(V_B, z) - P(0^+)}{P_s} - \alpha_{\text{tot},u}(V_B)z. \quad (19)$$

$P(V_B, z)$ in (19) satisfies with the following boundary conditions of

$$P(V_B, z = 0^+) = P_{\text{in}}C_{\text{input}}(1 - R_f) \quad (20)$$

$$P(V_B, z = L^-) = P_{\text{out}}(V_B)/C_{\text{output}}(1 - R_f). \quad (21)$$

The saturation power $P_s(V_B)$ is easily found by inserting the boundary conditions into (19).

$$P_s(V_B) = \frac{1 - T/K_p}{\alpha_{\text{tot},u}L + \ln(T/K_p)} C_{\text{input}}P_{\text{in}} \quad (23)$$

where T and K_p are defined in (5) and (7), respectively.

Analysis procedure for high optical input power is as follows: We obtain the total optical absorption coefficient $\alpha_{\text{tot},u}$, K_p , and C_{input} from the method explained in Section II-A. The saturation optical power $P_s(V_B)$ in (23) is found by using the measured transmission data $T(V_B)$. The power profile $P(V_B, z)$ inside device is known from the (19) and the total absorption coefficient $\alpha_{\text{tot}}(V_B, z)$ is calculated from (17).

III. EXPERIMENT AND DISCUSSIONS

We apply the method described in the previous section to find the changes of optical losses in our MQW EAM [20]. The MQW structure consists of ten tensile-strain wells (InGaAsP, -0.35% , 12 nm) and 11 compressive-strain barriers (InGaAsP, $+0.57\%$, 7 nm). The active region is sandwiched between p-InP and n-InP cladding layers. The total thickness of the intrinsic layer is about 300 nm. A 300- μm -long and 2- μm -wide ridge-waveguide device is fabricated. The optical confinement factor Γ is 0.2. The facets are coated by AR films. The device is mounted as the epi-side-up configuration on the

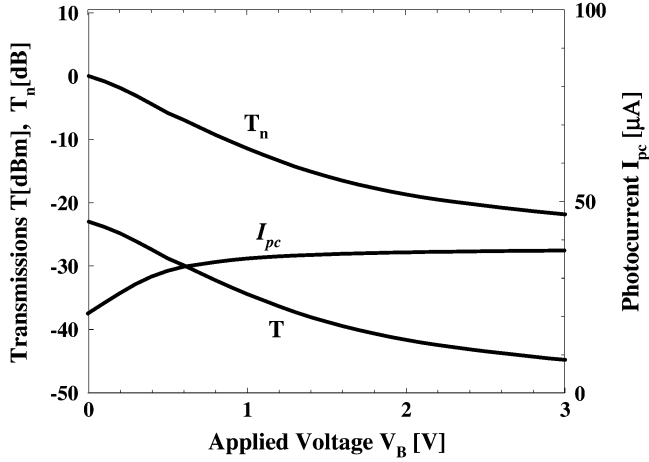


Fig. 1. Experimental data of the transmission T , normalized transmission T_n , and photogenerated current I_{pc} at $P_{in} = 250 \mu\text{W}$ as a function of bias voltage.

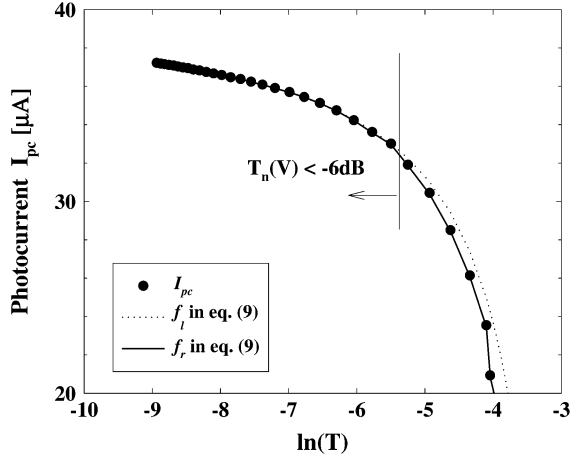


Fig. 2. Experimental data of photogenerated currents as a function of $\ln(T)$. The circle points are the redrawn experimental data I_{ph} from Fig. 1. The dashed and the straight lines correspond to the left and the right terms in (9) after converging process.

Cu sheet about $200 \mu\text{m}$ thick by using solder bump. A tunable laser is used as the input optical source. The laser wavelength is $1.553 \mu\text{m}$ with TM polarization. Two lensed fibers are used at input and output ports of an EAM for light coupling.

We apply the method shown in Section II-A, in order to identify an intrinsic loss α_i , the residual interband absorption $\alpha_{cv,o}(=\alpha_{cv}(V_B = 0))$, and optical coupling efficiencies $C_{input}(C_{output})$ between the fibers and EAM. The optical input power is set as small as $250 \mu\text{W}$ in order to minimize the saturation effect of an optical loss coefficient as well as the temperature increase due to the photocurrent. Fig. 1 shows the optical transmission T , the normalized transmission T_n and the photocurrent I_{pc} as a function of bias voltage V_B . Fig. 2 shows the three different photocurrents with respect to $\ln(T)$. The dotted points are the redrawn experimental data I_{pc} shown in Fig. 1. The straight and dashed lines correspond to the left and right terms in (9) after converging process. The least square method is used to obtain a, b , and c constants from the fitting. In the converging process, we assume that η_i is nearly one for $V_B \geq 1 \text{ V}$ which correspond to $T_n \leq -6 \text{ dB}$. It is clear that the left and right terms in (9) can be fitted very well for

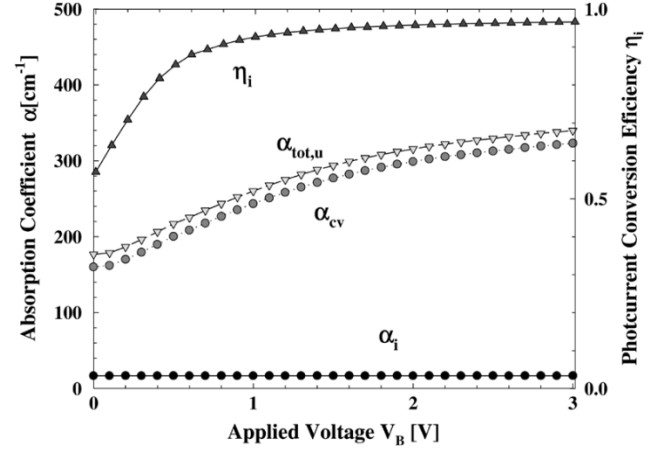


Fig. 3. Changes of optical losses and internal quantum efficiency η_i versus bias voltage V_B for the input light with $\lambda = 1553 \text{ nm}$ and $P_{in} = 250 \mu\text{W}$. $\alpha_i, \Gamma\alpha_{cv}$, and $\alpha_{tot,u}$ represent the absorption coefficient changes due to the intrinsic absorption, interband absorption, and the sum of both, respectively.

$T_n \leq -6 \text{ dB}$. However, the left and the right terms show a small discrepancy for $T_n > -6 \text{ dB}$ which implies that η_i can not be regarded as unity in a small bias region. The data of I_{ph} and the left term in (9) show almost the same values even in the range of $T_n \geq -6 \text{ dB}$. This implies that a measured EAM has a large residual loss satisfying with the condition of $e^{-(\alpha_i + \Gamma\alpha_{cv,o})L} \ll 1$.

Fig. 3 shows the calculated results of the unsaturated modal optical loss. The dependence of $\alpha_{tot,u}(=\alpha_i + \Gamma\alpha_{cv})$ on V_B is mainly determined by the interband absorption coefficient $\Gamma\alpha_{cv}$. There exists a large optical loss $\alpha_{tot,u}$ even at $V_B = 0 \text{ V}$, which consists of $\alpha_i = 17 \text{ cm}^{-1}$ and $\Gamma\alpha_{cv,o} = 160 \text{ cm}^{-1}$. Thus, in order to reduce the residual loss at $V_B = 0 \text{ V}$, the reduction of $\Gamma\alpha_{cv,o}$ is more important than that of α_i in this case. Fig. 3 also shows the change of $\eta_i(V_B)$. η_i slightly increases with V_B for $0 < V_B < 0.6 \text{ V}$ and remains a nearly one for $V_B \geq 0.6 \text{ V}$. Thus, we believe that a measured device is completely depleted for $V_B \geq 0.6 \text{ V}$. The total optical coupling loss $C_{input}C_{output}$ of 12 dB when $R_f = 0$ and K_p of 0.06 are estimated from the fitted parameter a in (11).

In contrast to the case of a low optical input power, the measured transmission data for a high input optical power involves the composite effects such as the exciton saturation, the charge buildup, and the device temperature variation. As an optical input power increases, both the exciton saturation effect and the photocurrent increase. A large photocurrent heats up the device by the Joule heating, which in turn changes absorption coefficient inside an EAM. We try to estimate the saturation of optical absorption coefficient for different optical input powers. In this analysis, the nonsaturated absorption coefficient $\alpha_{tot,u}(V_B)$ in (17) is assumed as the extracted values at $P_{in} = 250 \mu\text{W}$, which is shown in Fig. 3. It is preferred to use an optical input power as low as possible.

Figs. 4 and 5 show the optical output power P_{out} transmitted through the EAM and the photocurrent I_{ph} under the different optical power of input light and reverse bias voltages, respectively. Fig. 6 shows the longitudinal power distributions normalized at the powers at the input port, $P(V_B, z)/P(V_B, 0^+)$, at different bias voltages of 0 and 2 V for the optical input powers

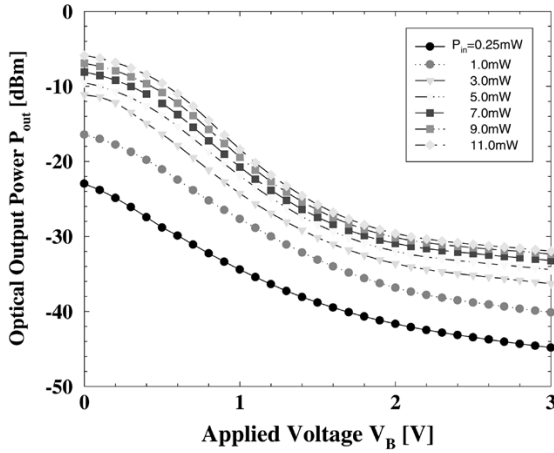


Fig. 4. Experimental data of optical output powers through an electroabsorption modulator as a function of bias voltage for the different input optical powers.

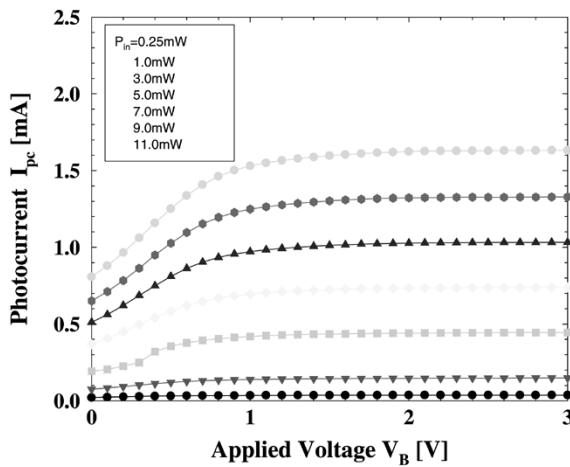


Fig. 5. Experimental data of photogenerated currents as a function of bias voltage for the different input optical powers.

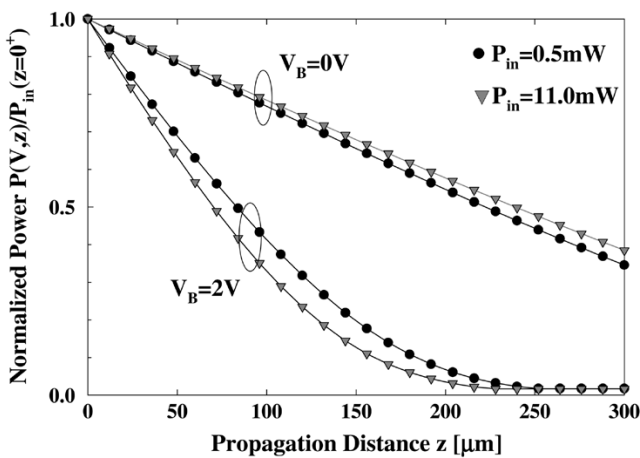


Fig. 6. Longitudinal power distribution normalized by the power at the input port. The modulator length is 300 μm .

of 0.5 and 11.0 mW. At $V_B = 0$ V, the optical absorption coefficient is not so large that the power almost linearly decreases as the light propagates. As an optical input power increases from 0.5 to 11 mW, the optical power absorption rate becomes

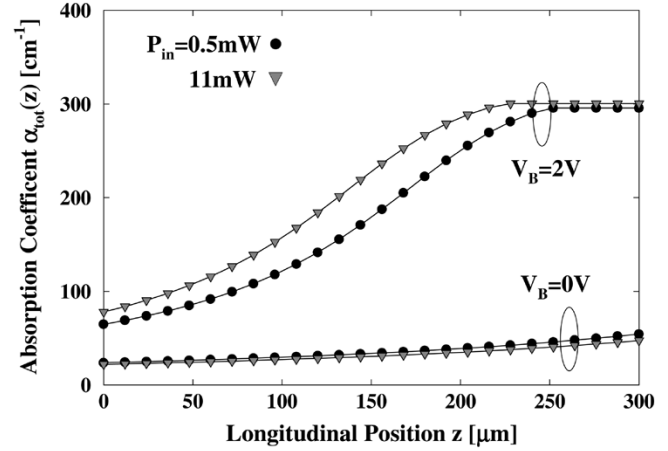


Fig. 7. Longitudinal distribution of absorption coefficient inside sample for different biases and input optical powers. The modulator length is 300 μm .

small. This means that the optical absorption coefficient for $P_{\text{in}} = 11$ mW is small compared to $P_{\text{in}} = 0.5$ mW. The saturation of absorption coefficient according to optical input power has been reported [12]–[15], [18], [19]. Several complex phenomena such as the band filling, charge buildup, and the field screening are in charge of the optical loss saturation in a low electric field. Those kinds of saturation effects bring to the transfer curve dependency on input optical power at low bias voltage like a $V_B = 0$ V since the electric field inside the device is not enough to sweep out the photogenerated carriers.

At $V_B = 2$ V, the optical power decreases more drastically compared to the case of zero bias voltage, which is due to a large optical absorption coefficient resulting from the QCSE. In our sample, optical powers are almost absorbed after propagating to about 250 μm regardless of optical input powers. However, the dependence of power distribution on optical input power is opposite to the zero bias case. This will be explained in the following temperature experiment. The longitudinal distribution of optical absorption coefficient will be inversely proportional to the longitudinal power profile as expected from (17). Fig. 7 shows the longitudinal distributions of optical absorption coefficients for different bias voltages and optical input powers. The absorption coefficient for $P_{\text{in}} = 11$ mW is larger than that for $P_{\text{in}} = 0.5$ mW at $V_B = 2$ V.

We estimate the amount of saturation effect in absorption coefficient as the factor of $P(V_B, z = 0^+)/P_s(V_B)$ for different optical input powers. $P(V_B, z)/P_s(V_B)$ accounts for the saturation effect in optical absorption coefficient along the propagation direction as shown in (17). Since optical power at $z = 0^+$ is the maximum inside device, the saturation effect will be greatest. Fig. 8 is the calculated result of $P(V_B, z = 0^+)/P_s(V_B)$ for different optical input powers. It is clear that the saturation effect increases with the optical input power at $V_B < 1$ V. However, an opposite trend appears at $V_B > 1$ V.

As previous discussions, the total optical loss $\alpha_{\text{tot}}(V_B)$ decreases with P_{in} for high bias voltages. This suggests that the exciton absorption peak broadening for high input optical power is large compared to the low input optical power. It is known that the broadening of an exciton absorption spectrum results from

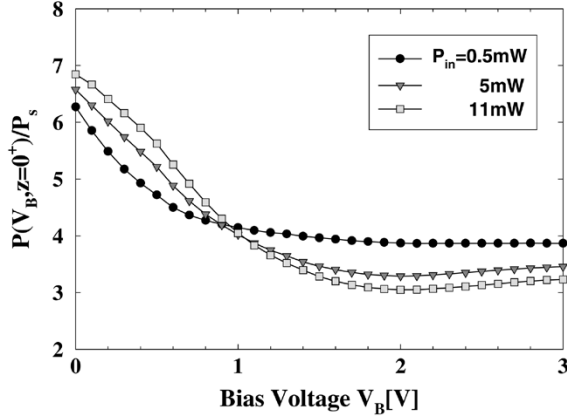


Fig. 8. Saturation of optical absorption coefficient for different biases and input optical powers. The modulator length is $300 \mu\text{m}$.

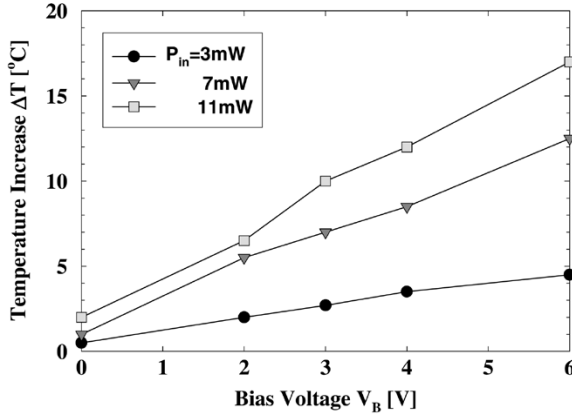


Fig. 9. Increase of modulator temperature due to the photogenerated current for different biases and input optical powers.

the increase of operating temperature as well as many-body effect due to large number of carriers in the wells. Since we are considering the situation in which an electric field in quantum wells is very high, total numbers of carriers in quantum wells are not so much different according to input optical powers. Therefore, the many-body effect does not seem to be a dominant exciton broadening mechanism in a high bias condition. Recently, Bian *et al.* measured the temperature in an EAM at different optical input powers and bias voltages [21]. Significant increase of the device temperature was observed even at a moderate input power of 6 mW as the bias voltage increased. We suspect that the major effect of the decrease in optical loss at a high bias region is due to temperature increase. The temperature increase is due to the large photogenerated current I_{ph} when an optical input power is high. In our EAM, I_{ph} is about $1\text{--}3 \text{ mA}$ for the measured condition of $V_B = 2 \text{ V}$ as shown in Fig. 5. Fig. 9 shows the measured temperature for different optical input powers. The temperature is measured around the input facet position by using the thermoreflectance technique, which is based on the temperature dependence of the surface reflection coefficient [21]. The significant temperature increase is observed for high input optical power. We believe that temperature effect is a dominant mechanism to produce the dependence of transfer curves on input optical power at $V_B = 2 \text{ V}$.

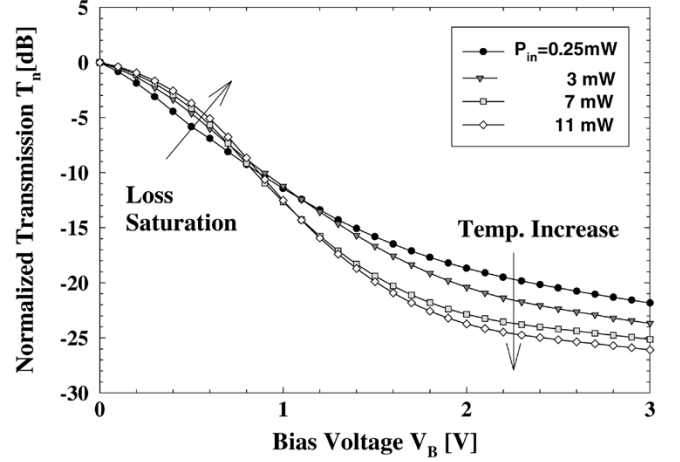


Fig. 10. Normalized transmission curve for different biases and input optical powers. The direction of transmission curve change and its dominant changing mechanisms are indicated at low and high bias regions separately.

Fig. 10 shows the transfer curves normalized at $V_B = 0 \text{ V}$ in order to show clearly the dependence of transfer curves on V_B and P_{in} . In $V_B \leq 1 \text{ V}$, the lower extinction ratio results from the optical loss saturation effects such as exciton saturation, band filling effect, and charge buildup. In $V_B \geq 1 \text{ V}$, the higher extinction ratio comes from the increase of device temperature by the photogenerated current from the higher input optical power. Thus, the reductions of both the band filling effect and device temperature increase are essential to decrease the dependence of transfer curves on the input optical power.

IV. CONCLUSION

We have presented a simple method to determine major physical parameters in an electroabsorption modulator such as the intraband optical loss coefficient, the interband optical loss coefficient, waveguide scattering loss, optical coupling efficiency, and the photocurrent conversion efficiency. This method uses only the measured transmission and photogenerated current data. It is effective when an optical input power is enough low that absorption coefficient inside sample is uniform. We further extended the analysis method of optical loss with optical input power dependence along the position. It is clarified that the dependence of transfer curves on input optical powers results from the optical loss saturation effect in the low bias region and the device temperature increase in the high bias region. The optical loss saturation was analyzed theoretically and the increase of the device temperature was verified experimentally. The proposed novel and simple optical loss measurement methods will be very useful for the design and optimization of an electroabsorption modulator.

ACKNOWLEDGMENT

The authors would like to thank Dr. Z. Bian and Dr. J. Christofferson in Prof. Ali Shakouri's group at University of California, Santa Cruz, CA, for the temperature measurement of EAMs.

REFERENCES

- [1] S. Kaneko, M. Node, Y. Miyazaki, H. Watanabe, K. Kasahara, and T. Tajime, "An electroabsorption modulator module for digital and analog applications," *J. Lightwave Technol.*, vol. 17, pp. 669–676, Apr. 1999.
 - [2] V. Kaman, Y. Chiu, T. Liljeberg, S. Z. Zhang, and J. E. Bowers, "Integrated tandem traveling-wave electroabsorption modulators for 100 Gbit/s OTDM applications," *IEEE Photon. Technol. Lett.*, vol. 12, pp. 1471–1473, Nov. 2000.
 - [3] W. S. C. Chang, *RF Photonic Technology in Optical Fiber Links*. Cambridge, U.K.: Cambridge Univ. Press, 2002.
 - [4] R. B. Welstand, S. A. Pappert, D. T. Nichols, L. J. Lembo, Y. Z. Liu, and P. K. L. Yu, "Enhancement in electroabsorption waveguide modulator slope efficiency at high optical power," *IEEE Photon. Technol. Lett.*, vol. 10, pp. 961–963, July 1998.
 - [5] B. W. Hakki and T. L. Paoli, "CW degradation at 300 K of GaAs double-heterostructure junction lasers-II: Electron gain," *J. Appl. Phys.*, vol. 44, pp. 4133–4119, 1973.
 - [6] D. Hofstetter and R. L. Thornton, "Measurement of optical cavity properties in semiconductor lasers by Fourier analysis of the emission spectrum," *IEEE J. Quantum Electron.*, vol. 34, pp. 1914–1923, Oct. 1998.
 - [7] D. A. Ackerman, L. M. Zhang, L. J.-P. Ketelsen, and J. E. Johnson, "Characterizing residual reflections within semiconductor lasers, integrated sources, and coupling optics," *IEEE J. Quantum Electron.*, vol. 34, pp. 1224–1230, July 1998.
 - [8] T. H. Wood, "Direct measurement of the electric-field-dependent absorption coefficient in GaAs/AlGaAs multiple quantum wells," *Appl. Phys. Lett.*, vol. 48, no. 21, pp. 1413–1415, May 1986.
 - [9] M. K. Chin, "A simple method using photocurrent and power transmission for measuring the absorption coefficient in electroabsorption modulators," *IEEE Photon. Technol. Lett.*, vol. 4, pp. 866–869, Aug. 1992.
 - [10] J. Piprek, *Semiconductor Optoelectronic Devices: Introduction to Physics and Simulation*. New York: Academic, 2002.
 - [11] M. Asada, K. Kameyama, and Y. Suematsu, "Gain and intervalence band absorption in quantum-well lasers," *IEEE J. Quantum Electron.*, vol. QE-20, pp. 745–753, July 1988.
 - [12] G. Livescu, D. A. B. Miller, D. S. Chemla, M. Ramaswamy, T. Y. Chang, N. Sauer, A. C. Gossard, and J. H. English, "Free carrier and many-body effects in absorption spectra of modulation-doped quantum wells," *IEEE J. Quantum Electron.*, vol. QE-24, pp. 1677–1689, Aug. 1988.
 - [13] J. Aristide, D. A. B. Miller, J. E. Chunningham, P. L. K. Wa, and A. Miller, "Simultaneous measurement of electron and hole sweep-out from quantum wells and modeling of photoinduced field screening dynamics," *IEEE J. Quantum Electron.*, vol. 28, pp. 2486–2497, Oct. 1992.
 - [14] A. M. Fox, D. A. B. Miller, G. Livescu, J. E. Cunningham, and W. Y. Jan, "Quantum well carrier sweep out: Relation to electroabsorption and exciton saturation," *IEEE J. Quantum Electron.*, vol. 27, pp. 2281–2295, Oct. 1991.
 - [15] M. Wiedenhaus, A. Ahland, D. Schulz, and E. Voges, "Modeling and simulation of electroabsorption modulators," *Inst. Elect. Eng. Proc. Optoelectron.*, vol. 149, no. 4, pp. 122–130, Aug. 2002.
 - [16] A. Alping, R. Tell, and S. T. Eng, "Photodetection properties of semiconductor laser diode detectors," *J. Lightwave Technol.*, vol. LT-4, pp. 1662–1668, Nov. 1986.
 - [17] J. Harari, F. J. Jourmet, O. Rabii, G. Jin, J. P. Vilcot, and D. Descoster, "Modeling of waveguide PIN photodetectors under very high optical power," *IEEE Trans. Microwave Theory Tech.*, vol. 43, pp. 2304–2209, Sept. 1995.
 - [18] P. J. Bradley, C. Rigo, and A. Stano, "Carrier induced transient electric fields in a p-i-n InP-InGaAs multiple-quantum-well modulator," *IEEE J. Quantum Electron.*, vol. 32, pp. 43–52, Jan. 1996.
 - [19] D. S. Chemla, D. A. B. Miller, P. W. Smith, A. C. Gossard, and W. Wiegmann, "Room temperature excitonic nonlinear absorption and refraction in GaAs–AlGaAs multiple quantum well structures," *IEEE J. Quantum Electron.*, vol. QE-20, pp. 265–275, Mar. 1984.
 - [20] Y. Chiu, V. Kaman, S. Z. Zhang, and J. E. Bowers, "Distributed effects model for cascade traveling-wave electroabsorption modulator," *IEEE Photon. Technol. Lett.*, vol. 13, pp. 791–793, Aug. 2001.
 - [21] Z. Bian, J. Christofferson, A. Shakouri, and P. Kosedoy, "High power operation of electroabsorption modulators," in *Proc. Conf. Dig., CLEO/QELS*, Baltimore, MD, 2003, Paper CtuJ5.
- Jongin Shim** (M'95) was born in Kangreung, Korea, in 1960. He received the B.S. and M.S. degrees in electronics from the Seoul National University, Seoul, Korea, in 1983 and 1985, respectively and the Ph.D. degree in physical electronics from the Tokyo Institute of Technology, Tokyo, Japan, in 1992. His Ph.D. dissertation was mainly concerned with static and dynamic properties of single mode lasers such as DR, DBR, and DFB lasers.
- From 1985 to 1988, he worked in Electronics and Telecommunication Research Institute (ETRI), Taejeon, Korea, on InGaAsP–InP semiconductor lasers. From 1992 to 1994, he joined Optoelectronics Research Laboratory of NEC, Tsukuba, Japan, where he conducted research on tunability and coherence of semiconductor lasers and their fabrication technology by the selective metal–organic vapor phase epitaxy (MOVPE) growth. He is currently with the Department of Electronics, Hanyang University, Korea, as a Professor. His primary interests are microwave and photonic devices for optical communication.
- Dr. Shim received an Excellent Student Award in 1992 from the Tokyo Institute of Technology.
- Bin Liu** received the B.S. degree from Zhejiang University, Zhejiang, China, in 1990, the M.S. degree from Shanghai Institute of Optics and Fine Mechanics, Chinese Academy of Science, Shanghai, China, in 1995, and the Ph.D. degree in electrical engineering from the University of California, Santa Barbara, in 2000.
- He is currently with LuminentOIC Inc. and developing optical devices for FTTP application. His research interests include the design and fabrication of semiconductor optical waveguide devices, lasers, photonic integrated circuits, and microoptic devices.
- John E. Bowers** (M'81–SM'85–F'93) received the M.S. and Ph.D. degrees from Stanford University, Stanford, CA, in 1978 and 1981, respectively.
- He is Director of the Multidisciplinary Optical Switching Technology Center (MOST), and a Professor in the Department of Electrical Engineering, University of California, Santa Barbara. His research interests are primarily concerned with optoelectronic devices and optical networking. He is cofounder of the Center for Entrepreneurship and Engineering Management, and a cofounder of Terabit Technology and Calient Networks. He worked for AT&T Bell Laboratories and Honeywell before joining UCSB. He has published 6 book chapters, 350 journal papers, 600 conference papers, and has received 32 patents.
- Dr. Bowers is a fellow of the OSA and the American Physical Society, and a recipient of the IEEE LEOS William Streifer Award and the South Coast Business and Technology Entrepreneur of the Year Award.